Heliyon 11 (2025) e41295

Contents lists available at ScienceDirect

Heliyon

journal homepage: www.cell.com/heliyon

Research article

Leveraging RIBOTAC technology: Fluorescent RNase L probes for live-cell imaging and function analysis

Elias Khaskia , Raphael I. Benhamou *

The Institute for Drug Research of the School of Pharmacy, Faculty of Medicine, The Hebrew University of Jerusalem, Jerusalem, Israel

ARTICLE INFO

Keywords:
RIBOTAC
RNase L
Fluorescent probes
Subcellular localization

ABSTRACT

RNA-targeting small molecules, particularly RIBOnuclease TArgeting Chimeras (RIBOTACs), represent a powerful and promising therapeutic approach by selectively degrading RNAs through ribonuclease (RNase) recruitment. Despite their potential, the development of effective RNase recruitment tools is still in its early stages and remains a critical area of research. Ribonuclease L (RNase L) is a key ribonuclease targeted by RIBOTACs, yet the tools available for studying RNase L are limited. In this study, we introduce novel fluorescent ribonuclease binders that enhance the visualization and investigation of RNase L activity. Our findings provide new insights into RNase L dynamics and RNA degradation pathways, paving the way for more effective RNA-targeted degradation strategies. Furthermore, we explore the versatility of these conjugates for real-time tracking of RNase L localization, intracellular trafficking, and mechanistic studies. These fluorescent probes also enable high-throughput fluorescence-based assays to identify small molecules that bind and recruit RNase L, advancing RNA-targeted therapeutic approaches.

1. Introduction

Ribonuclease L (RNase L), a key enzyme in the antiviral defense mechanism of cells, is an endoribonuclease activated through the interferon pathway [1]. It plays a crucial role in restricting the replication of various viruses, such as influenza, chikungunya, SARS-CoV-2, and vaccinia in mammals [2–4]. Activation of RNase L occurs when oligoadenylate synthetase system (OAS) polymerizes ATP into 2′,5′-oligoadenylates (2–5A). These 2–5A molecules subsequently bind to monomeric RNase L, inducing its dimerization and subsequent catalytic activity presented in cleaving single-stranded RNA (ssRNA) at UU/UA motifs, resulting in dsRNA cleavage products with 5′-hydroxyl and 2′,3′-cyclic phosphate ends [5–7]. This process is a part of the broader 2–5A system, which is essential for controlling viral infections and modulating immune responses (Fig. 1A) [1,8]. Despite the well-established role of RNase L in antiviral defense, the real-time dynamics and intracellular behavior of RNase L during RNA degradation remain inadequately explored. Current methodologies fall short of providing real-time visualization of RNase L activation and subsequent RNA degradation pathways [9–11]. Therefore, it is necessary to develop methods that can overcome these obstacles and enable detailed studies of RNase L dynamics and functions within the cellular environment.

Notably, the recruitment of RNase L has been used to target and degrade disease-associated RNAs [12]. This effective strategy, known as RIBOnuclease TArgeting Chimera (RIBOTAC), has proven highly potent in reducing toxic RNAs [13]. In this context, RNase L is an attractive ribonuclease because it is an endoribonuclease that is activated only when dimerized and fits well within the field of

* Corresponding author.
E-mail address: raphael.benhamou@mail.huji.ac.il (R.I. Benhamou).

https://doi.org/10.1016/j.heliyon.2024.e41295
Received 29 August 2024; Received in revised form 8 December 2024; Accepted 16 December 2024
Available online 19 December 2024

small molecule targeting RNA, as it is capable of cleaving UN unpaired bases [5,6]. Recently, two small molecules, Ribo1 and Ribo2 (Fig. 1B), were developed to recruit RNase L and were conjugated to RNA small molecules [14,15]. RIBOTACs are a novel class of molecules in drug discovery that enable precise degradation of disease-related RNAs by recruiting RNase L to specific RNA targets [16–19]. This approach provides significant importance, including enhanced specificity and minimized off-target effects, making RIBOTACs highly effective in reducing pathogenic RNA involved in diseases like cancer and viral infections [20,21]. The dual functionality of RIBOTACs, binding to RNA and inducing its degradation via dimerization of RNase L, allows for controlled modulation of RNA levels [14], which is crucial for therapeutic efficacy (Fig. 1B). Additionally, their ability to selectively target RNA offers a powerful tool for managing diseases at the RNA level, providing a promising strategy for therapeutic interventions [22]. However, this method is still in its infancy, and more needs to be understood about the recruitment of RNase L and other ribonucleases. Further development of additional recruiters is necessary to advance this approach.

A variety of assays have been developed to study RNase activity, each with distinct strengths and limitations. For example, gel-based assays are cost-effective but limited to qualitative data, while FRET probes provide sensitive, real-time detection but require precise design and are sensitive to environmental conditions [23,24]. Immunoassays like ELISA offer high specificity yet typically detect RNase presence rather than activity [25]. Recently, fluorescent probes based on small molecules have been extensively used with fluorescence imaging techniques to track molecular events in living cells [26]. This non-invasive approach allows for in situ detection of various biomolecules [27]. These probes offer several advantages: small, easy to handle, chemically stable, and minimally perturb native functions [28]. Their flexibility in design and application makes them ideal for labeling at the cellular level, enabling a detailed understanding of cellular structure, localization, dynamics, and intracellular interactions [29].

Building upon the foundation of RNase L activation and the innovative development of RIBOTACs, we have advanced this approach by conjugating ribonuclease recruiters to various fluorescent probes including Diethylamino Coumarin (Cou), Fluorescein (Fluo), Nitrobenzodiazole (NBD), and Cyanine-5 (Cy-5). This modification leverages the advantages of fluorescence imaging techniques, providing a non-invasive and sensitive method to track molecular events in living cells. By employing these fluorescently labeled recruiters, we achieved real-time visualization of their localization and dynamics within cellular environments, enabling detailed studies of intracellular trafficking and mechanisms of action. Additionally, this approach allows us to investigate RNase L dynamics and its influence on RNA degradation pathways, offering valuable insights for potential therapeutic applications.

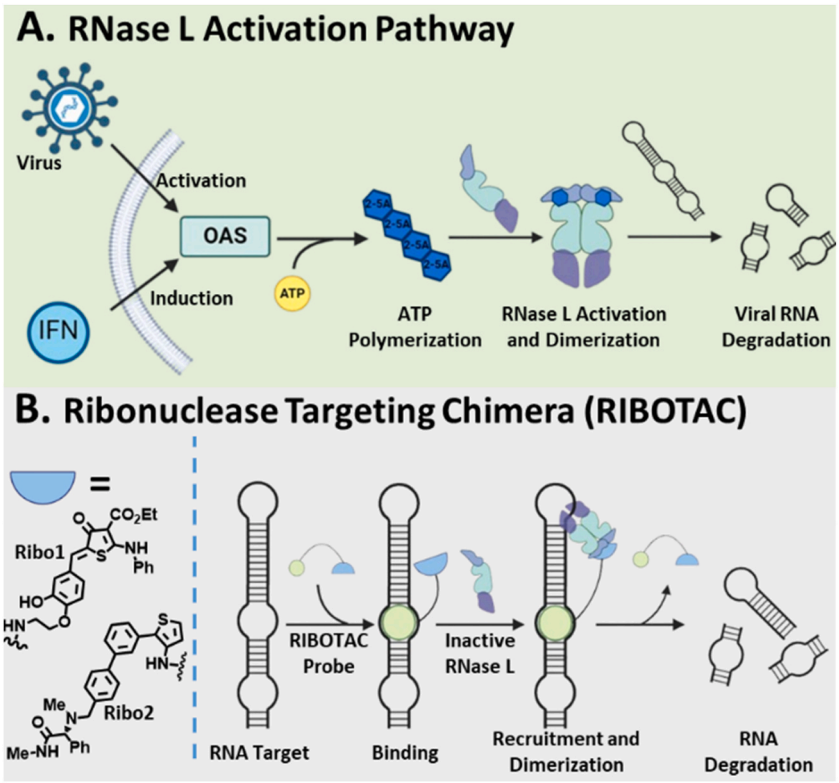

Fig. 1. RNase L activation. A) IFN-induced RNase L activation pathway. B) RIBOnuclease TArgeting Chimera strategy for degrading target RNA.

2. Methods

2.1. Preparation of RNase L-GST protein

RNase L-GST protein was purchased from Gene-Script company (Lot: U282HCNSG0-8/P2IH001), expression host: *E. coli*, purification: Protein was obtained from the supernatant of cell lysate, GST column + Superdex 200 column, purity: ≥80 % (SDS-PAGE under reducing condition, storage: 40 mM HEPES, 140 mM NaCl, 4 mM $MgCl_2$, 2 mM DTT, 30 % Glycerol, pH 7.4).

Protein Length = 741 MESRDHNNPQEGPTSSSGRRAAVEDNHLLIKAVQNEDVDLVQQLLEGGANVNFQEEEGGWTPLHNAVQMSRE
DIVELLLRHGADPVLRKKNGATPFILAAIAGSVKLLKLFLSKGADVNECDFYGFTAFMEAAVYGKVKALKFLYKRGANVNLRRKTKEDQERLRK
GGATALMDAAEKGHVEVLKILLDEMGADVNACDNMGRNALIHALLSSDDSDVEAITHLLLDHGADVNVRGERGKTPLILAVEKKHLGLVQRL
LEQEHIEINDTDSDGKTALLLAVELKLKKIAELLCKRGASTDCGDLVMTARRNYDHSLVKVLLSHGAKEDFHPPAEDWKPQSSHWGAALKDLH
RIYRPMIGKLKFFIDEKYKIADTSEGGIYLGFYEKQEVAVKTFCEGSPRAQREVSCLQSSRENSHLVTFYGSESHRGHLFVCVTLCEQTLEACLDV
HRGEDVENEEDEFARNVLSSIFKAVQELHLSCGYTHQDLQPQNILIDSKKAAHLADFDKSIKWAGDPQEVKRDLEDLGRLVLYVVKKGSISFED
LKAQSNEEVVQLSPDEETKDLIHRLFHPGEHVRDCLSDLLGHPFFWTWESRYRTLRNVGNESDIKTRKSESEILRLLQPGPSEHSKSFDKWTTKI
NECVMKKMNKFYEKRGNFYQNTVGDLLKFIRNLGEHIDEEKHKKMKLKIGDPSLYFQKTFPDLVIYVYTKLQNTEYRKHFPQTHSPNKPQCD
GAGGASGLASPGC.

2.2. Cell lines

Compounds were tested in MDA-MB-231 and MCF-7 human breast adenocarcinoma cell lines (HTB-26; ATCC, and HTB-22; ATCC respectively), and HEK-293 human embryonic kidney cell line (CRL-1573; ATCC).

2.3. Cell culture

All cells were maintained at 37 °C with 5 % CO_2. MCF-7 and HEK-293 cells were cultured in DMEM medium with L-Glutamine, 10 % (v/v) fetal bovine serum (FBS; Sigma-Aldrich; F9665) and 1 % (v/v) penicillin/streptomycin solution (Diagnovum; D910). MDA-MB-231 cells were cultured in RPMI 1640 medium with L-Glutamine supplemented with 25 mM HEPES (Capricorn Scientific; HEP-B), 10 % (v/v) FBS, and 1 % (v/v) penicillin/streptomycin solution. 22RV1 cells were cultured in F12K medium with L-Glutamine, 10 % (v/v) FBS, and 1 % (v/v) penicillin/streptomycin solution.

2.4. Resazurin cell viability assay

MCF-7 cells at 80 % confluence in 96-well plates were treated with synthesized compounds with different concentrations for 24 h. The resazurin assay kit (Abcam, ab129732) was used to analyze cell viability by incubating each sample with 20x cell viability solution for 4 h before fluorometric analysis. The fluorescence resulting from resazurin reduction to resorufin was measured with excitation and emission wavelengths of 530 and 570 nm, respectively, using the Synergy H1 Hybrid Multi-Mode Microplate Reader (BioTek, Agilent). Cell viability was calculated as the percent increase in fluorescence of treated cells compared to fluorescence in untreated cells.

2.5. Western blotting

MCF-7, MDA-MB-231, 22RV1, and HEK-293 cells were grown in 6-well plates at about 60 % confluency in a complete growth medium and the cells were left to grow to about 80 % confluency. Total protein was extracted using RIPA cell lysis buffer (BioPrep) containing protease inhibitor, and protein concentration was measured using BCA protein assay (Sigma-Aldrich) according to the manufacturer's protocol. Approximately, 50 μg of total protein was resolved on a 10 % SDS-acrylamide gel and then transferred to a PVDF membrane (Immobilon FL transfer membrane- Merck). The membrane was washed with 1x Tris-buffered saline (TBS) containing 0.1 % (v/v) Tween-20 (TBST; Tris-base, pH 7.6, NaCl, and Tween-20), and then blocked in 1x TBST containing 5 % (w/v) milk for 2 h at room temperature. The membrane was then incubated with 1:1000 dilution of rabbit anti-RNase L (Cell Signaling Technology: D4B4J), or 1:10,000 dilution of rabbit anti-Vinculin (Cell Signaling Technology: CS13901) in 1x TBST containing 5 % (w/v) milk overnight at 4 °C. The membrane was then washed three times (10 min per wash) with 1x TBST and incubated with 1:10,000 anti-rabbit IgG horseradish-peroxidase secondary antibody conjugate (Cell Signaling: CS7074) at room temperature for 2 h. After washing three times with 1x TBST (10 min per wash), the target protein was detected using ClearBand ECL Substrate (Gene Bio-Application) on Azure C300 Imaging System. The difference in expression of the target protein (RNase L) in the different cell lines was calculated by normalizing the band intensity to the vinculin band intensity using ImageJ.

2.6. In-vitro RNA cleavage

An RNA degradation assay was conducted by monitoring the decrease in intensity of FAM-labeled RNA on an SDS gel. Briefly, Ribo1, Ribo2, Ribo1-Cy5, Ribo2-Cy5, or Cy5-Ctrl were added to RNase L in a 1x activation buffer (containing 7 mM β-mercaptoethanol, 50 μM ATP, and 1 mM $MgCl_2$), heated at 95 °C for 5 min, then rapidly cooled on ice for 5 min. Following this, the mixture was incubated with FAM-labeled RNA for 2 h. Samples were subsequently loaded onto a 20 % SDS-polyacrylamide gel. Band intensities were detected using the ChemiDoc MP Imaging System (Bio-Rad) and analyzed in ImageJ by normalizing each band intensity to that of

the RNA-alone control. RNA sequence that has been used in this study 5′-FAM-r(UUAGGGUUAGGGUUAGGGUUAGGG)-3' (Integrated DNA technologies).

2.7. Evaluation of excitation and emission maxima and determination of concentration

Synthesized compounds were subjected to spectral scanning in different concentrations using 96-well plates. Maximum excitation and emission wavelengths were measured using the Synergy H1 Hybrid Multi-Mode Microplate Reader (BioTek, Agilent). Wells containing DDW were added for background subtraction purposes.

2.8. Fluorescence binding assay

Half-maximal effective concentration (EC_{50}) measurements between synthesized compounds and RNase L protein were performed by detecting the difference in fluorescence intensity as a function of protein concentration. In short, the protein was folded in 1x Binding buffer (8 mM Na_2HPO_4, pH 7.0, 185 mM NaCl, and 1 mM EDTA) at 95 °C for 5 min and then cooled on ice for an additional 5 min. Compound solutions were prepared in 1x Binding buffer. The protein of interest was titrated into these solutions, starting from 5 nM and diluted with a dilution factor of 2 down to 2.44 pM (12 concentrations in total). The mixtures were then incubated at 37 °C for various time points in 96-well plates. Plots of protein concentration versus changes in fluorescence were used to determine EC_{50} values, measured using the Synergy H1 Hybrid Multi-Mode Microplate Reader (BioTek, Agilent).

2.9. Competition assay

Binding site validation assays were performed by detecting differences in fluorescence intensity as a function of increasing concentrations of RNase L recruiters lacking fluorophore conjugation (compounds **Ribo1** and **Ribo2**). In short, the protein was folded in 1x Binding buffer (8 mM Na_2HPO_4, pH 7.0, 185 mM NaCl, and 1 mM EDTA) at 95 °C for 5 min and then cooled on ice for an additional 5 min, followed by incubation with increasing concentrations of **Ribo1** or **Ribo2** for 10 min at 37 °C. Synthesized compounds were then added to the mixture at a constant concentration and re-incubated for different time periods for each compound. Bar graphs were utilized to present the differences in fluorescence intensity measured using the Synergy H1 Hybrid Multi-Mode Microplate Reader (BioTek, Agilent).

2.10. Fluorescence microscopy

2.10.1. Compound localization and uptake evaluation

Compound localization and uptake evaluation were performed by detecting the compound's emission in a live-cell imaging assay. MCF-7 and MDA-MB-231 cells were seeded in μ-Slide 8 Well ibiTreat (© ibidi GmbH Cat.No:80826) at 5-11 $\times$ 10^4 cells/mL confluency. μ-Slide were previously treated with 10 % PDL in DDW (300 μL) for 1 h at 37 °C and washed with DDW (300 μL) three times. After cells reached 80 % confluency, treatments were performed with Ribo1-Cy5 (1 μM), Ribo2-Cy5 (1 μM), or Cy5-trl (1 μM) and incubated at 37 °C for either 5 min, 2 h, or 24 h. Cells were then washed three times with PBS and imaged using a NIKON New AX-R Confocal microscope at 60x magnification. Images were analyzed and presented using NIS-Elements AR 5.2.

2.10.2. Antibodies-based RNase L co-localization

MCF-7 cells were seeded onto glass coverslips in a 12-well plate. Upon reaching 80 % confluency, the cells were treated with either Cy5-Ctrl (0.1 μM), Ribo1-Cy5 (0.1 μM), or Ribo2-Cy5 (0.1 μM) for 2 h. Following treatment, the cells were washed three times with PBS and fixed with 4 % PFA (500 μL) in PBS for 10 min at room temperature, followed by three washes with ice-cold PBS. The cells were then permeabilized with 0.2 % Triton X-100 in PBS for 10 min at room temperature, followed by three washes with PBS. Blocking was performed using 500 μL of blocking buffer composed of 1 % BSA and 22.52 mg/mL glycine in PBST (PBS + 0.1 % Tween 20) for 2 h at room temperature. The cells were then incubated with Mouse Anti-RNase L Monoclonal Primary Antibody (E−9) (Santa Cruz, Cat. SC-74405, 1:100 dilution in 1 % BSA in PBST) for 1 h at room temperature, followed by an overnight incubation at 4 °C. The next day, the cells were washed three times with PBS for 5 min each and incubated with the secondary antibody Goat Anti-Mouse IgG H&L Alexa Fluor® 488 (Abcam, Cat. AB-ab150113, 1:750 dilution in 1 % BSA in PBS) for 1 h at room temperature. The cells were then washed three times with PBS for 5 min each, followed by mounting with Prolong Gold Antifade Reagent with DAPI (Cell Signaling, Cat. 8961S) and sealing the coverslips with nail polish. The slides were imaged using a NIKON New AX-R Confocal microscope at 60x magnification. Images were analyzed and processed using NIS-Elements AR 5.2.

2.10.3. Plasmid-based RNase L co-localization

For this RNase L co-localization assay, we used a plasmid from GeneCopoeia (OmicsLink™ Expression Clone (EX-U1047-M29; GeneCopoeia, Inc., Rockville, MD)), containing a Homo sapiens RNase L gene tagged with GFP, with a total size of 8390 base pairs. The plasmid is constructed in the pEZ-M29 vector, has an accession number of NM_021133, and confers ampicillin resistance. MCF-7 cells were seeded into a 96-well plate. Upon reaching 80 % confluency, the cells were transfected with 0.5 μg of the plasmid using a 1:5 ratio of the PEI transfection reagent (Med Chem Express, HY-K2014) at a concentration of 1 mg/mL, following the manufacturer's protocol. After 24 h of transfection, the cells were transferred to PDL-treated μ-Slide 8 Wells. Following a 12-h incubation, the cells were treated with either Cy5-Ctrl (0.1 μM), Ribo1-Cy5 (0.1 μM), or Ribo2-Cy5 (0.1 μM) for 2 h. The cells were then washed three times with PBS and

incubated with DAPI (1 μg/mL, 300 μL) for 10 min at 37 °C, followed by another three washes with PBS. Imaging was performed using a NIKON New AX-R Confocal microscope at 60x magnification. Images were analyzed and presented using NIS-Elements AR 5.2.

2.10.4. Flow cytometry

Compound uptake evaluation was performed by flow cytometry using a CytoFLEX Flow Cytometer (Beckman Coulter, Rhenium). MCF-7, MDA-MB-231, 22RV1, and HEK-293 cells were seeded into 6-well plates. After reaching 80 % confluency, the cells were treated with Ribo1-Cy5 (1 μM), Ribo2-Cy5 (1 μM), or Cy5-Ctrl (1 μM) and incubated at 37 °C for either 5 min, 2 h, or 24 h. Cells were washed with PBS three times for 5 min each, filtered using a cell strainer (70 μm), and subjected to the CytoFLEX cytometer for uptake evaluation. Analysis was performed using FlowJo software (FlowJo_v10.10).

2.11. Quantification and statistical analysis

Standard deviation (SD), standard error of the mean (SEM), and One-way ANOVA were done using GraphPad Prism 10 software. Pearson's Correlation was done using ImageJ software. Statistical details for each experiment can be found in the figure legends and the detailed methods for each experiment.

3. Results

3.1. Synthesis of the fluorescent probes

To study RNase L, we have developed several fluorescent probes capable of binding RNase L. These probes are based on previously reported RNase L recruiters used in the development of RIBOTAC molecules. Ribo1 was discovered by Silverman et al. [30] to bind and dimerize RNase L, while Ribo2 was identified by Disney et al. [15] using a DNA-encoded library and was further designed into RNA degrader conjugates. To cover most of the visible light spectrum and develop various fluorescent tools, we conjugated the two RNase L recruiters with different fluorophores. The positions used for conjugating the fluorophores are the same positions used for adding the small molecule binding RNA in the RIBOTAC approach, ensuring that the binding to RNase L is not affected. For the blue wavelength range, we used a Coumarin molecule. For the green range, we employed two different fluorophores: Fluorescein and NBD. Finally, to cover the red spectrum, we conjugated the recruiters with a Cy5 molecule (Fig. 2). The purity of the compounds was evaluated using analytical HPLC (Fig. S1), and each fluorescent probe's absorbance and emission spectra were also assessed (Fig. S2). Overall, the emission of these probes spans from approximately 470 nm for the Coumarin derivatives, to around 520 nm for Fluorescein, approximately 560 nm for NBD, and up to 665 nm for the Cy5 probes.

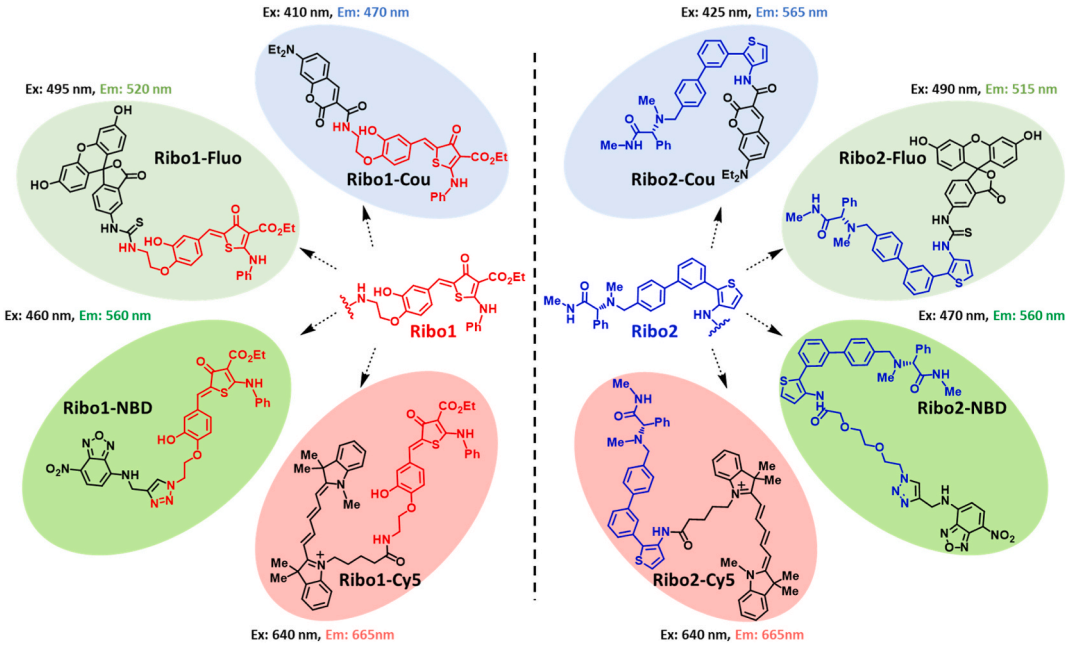

Fig. 2. Fluorescent RNase L probes. The Ribo1 binder is shown in red, and the Ribo2 binder is shown in blue. Four families of fluorophores were synthesized and are highlighted with different backgrounds: Diethylamino Coumarin (blue), Fluorescein (light green), Nitrobenzodiazole (NBD) (dark green), and Cyanine-5 (red).

3.2. Binding evaluation reveals fluorescence shifts in RNase L probes with varying affinities

As a first step in validating that the fluorescent probes are indeed binding RNase L, we proceeded with the evaluation of their affinity. We utilized the intrinsic fluorescence capacity of the probes and measured the change in fluorescence upon binding. It is known that when stabilized due to binding to another molecule, fluorophores will exhibit a change in their fluorescence [31]. However, whether this change results in an increase or decrease in fluorescence can be unpredictable, depending on the spatial orientation of the fluorophore relative to the protein. These orientations can influence the local environment surrounding the fluorophore, including interactions with nearby amino acid residues, quenching effects, or shifts in energy transfer efficiency. The probes were maintained at a constant concentration, while RNase L was added at various concentrations to generate a binding curve. Upon RNase L binding, a decrease in fluorescence was observed for the Cy5 derivatives (Ribo1-Cy5 and Ribo2-Cy5) and the NBD derivative (Ribo2-NBD) (Fig. 3A, B, and 3H). In contrast, an increase in fluorescence was noted for the Fluorescein derivatives (Ribo1-Fluo and Ribo2-Fluo) and the Coumarin derivative (Ribo2-Cou) (Fig. 3C, D, and 3F). Of note, Ribo1-NBD, Ribo2-Cou, and controls did not show proper saturation in fluorescence changes at the tested concentrations and were therefore considered not to exhibit binding to RNase L in this range of concentrations (Fig. 3E and G, and S3). Importantly, the EC_{50} values observed, which indicate the avidity of the probes to bind RNase L, were in the high picomolar range.

3.3. Validation of fluorescent probes for RNase L binding sites via competitive assays

To assess whether the designed fluorescent probes target the same binding site on RNase L as the original RNase L binders, Ribo1 and Ribo2, we conducted a competitive binding assay. In this assay, the parental RNase L binders were used at increasing concentrations, while the concentrations of the fluorescent probes and RNase L were kept constant. Although complete competition between the fluorescent probes and the parental binders Ribo1 and Ribo2 does not definitively rule out allosteric effects, it is worth noting that the structure of the fluorescent probes is derived directly from the parent binders; each probe incorporates the same core binding elements conjugated with a fluorophore. This structural overlap makes it more likely that competition arises from shared binding sites rather than allosteric regulation. Nonetheless, we acknowledge the possibility that binding may involve allosteric influences, where the interaction of one probe could alter RNase L's conformation to affect the binding of another. Notably, several fluorescent probes demonstrated complete competition with the parental binders, validating that they share the same RNase L binding pocket. The two Cy5 derivatives, Ribo1-Cy5 and Ribo2-Cy5 were 100 % validated (Fig. 4A, B, 4C, and 4D) along with Ribo2-Cou derivative (Fig. 4E and F). Finally, Ribo2-Fluo and Ribo2-NBD were validated with Ribo2 competition. Throughout the experiment, the fluorescence pattern exhibited a continuous and consistent decrease for Ribo2-Fluo (Fig. S4D) and an increase for Ribo2-NBD (Fig. S4F). The fluorescence pattern was less continuous and consistent for Ribo2-Fluo and Ribo2-NBD competition with Ribo1 (Figs. S4C and S4E). We hypothesize that Ribo1 may disrupt and affect the emission of these two probes likely because it is not the parental competitor. The other probes did not show full competition with the parental binders (Figs. S4A and S4B). Interestingly, not all the fluorescent probes exhibited proper fluorescence reversion. This could be due to binding to different binding pockets of the compounds or interactions between Ribo1 and Ribo2 with the evaluated fluorescent probes, which can affect the fluorescence change observed when unbinding or binding RNase L. Remarkably, the probes coupled to Ribo2 exhibited the most robust binding and validation rates.

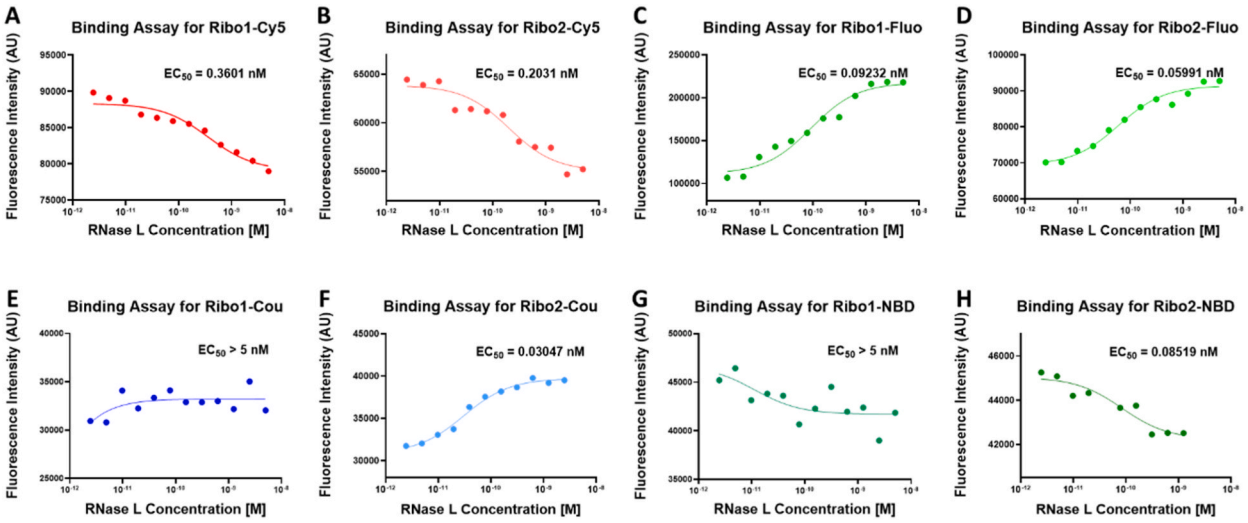

Fig. 3. Fluorescence-based binding assay. RNase L was titrated into a constant concentration of each derivative and was incubated at 37 °C. The EC_{50} values for each probe are annotated above their respective binding curves. A) Ribo1-Cy5 (20 μM). B) Ribo2-Cy5 (20 μM). C) Ribo1-Fluo (50 μM). D) Ribo2-Fluo (2 μM). E) Ribo1-Cou (12.5 μM). F) Ribo2-Cou (12.5 μM). G) Ribo1-NBD (80 μM). H) Ribo2-NBD (80 μM).

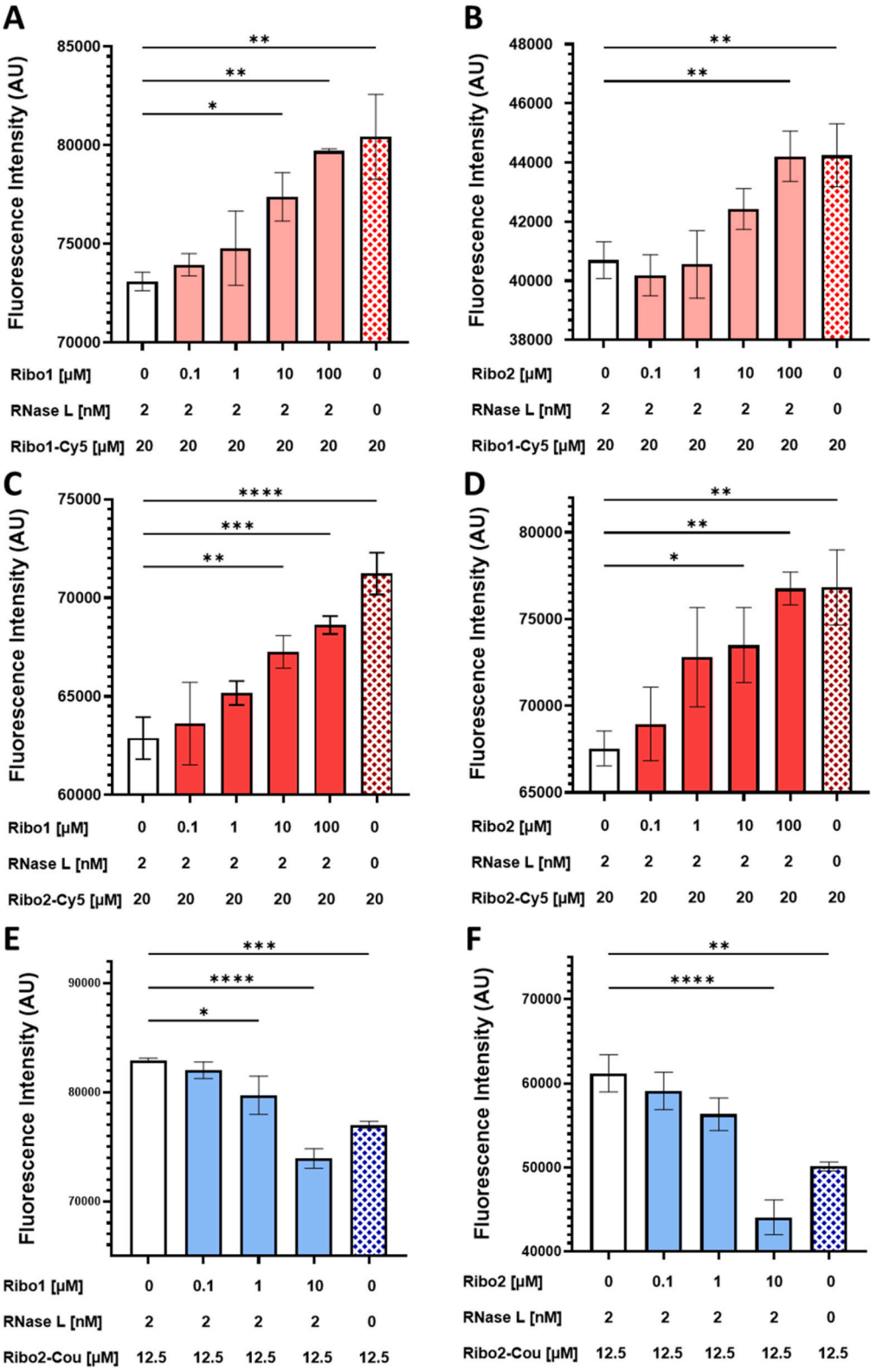

(caption on next page)

Fig. 4. Fluorescent-based competition assay for target validation. RNase L was incubated with increasing concentrations of Ribo1 or Ribo2 for 10 min at 37 °C, followed by incubation with the fluorescent probes for another 2 h. A) Competition between Ribo1-Cy5 and Ribo1. B) Competition between Ribo1-Cy5 and Ribo2. C) Competition between Ribo2-Cy5 and Ribo1. D) Competition between Ribo2-Cy5 and Ribo2. E) Competition between Ribo2-Cou and Ribo1. F) Competition between Ribo2-Cou and Ribo2. Statistical analysis was performed using one-way ANOVA test. Error bars represent the SD of the mean (n = 3). ** represents $P \leq 0.01$, *** represents $P \leq 0.001$ and **** represents $P \leq 0.0001$.

3.4. In-vitro RNase L activation and RNA degradation

To evaluate whether RNase L retains its activity when bound to Ribo1-Cy5 or Ribo2-Cy5, we performed an in vitro RNA degradation assay. In this assay, RNase L was pre-incubated with each compound in an activation buffer and then allowed to react with FAM-labeled RNA for 2 h. Incubation of RNase L with the parent recruiters, Ribo1 and Ribo2, led to a decrease in FAM intensity by approximately 45 % and 25 %, respectively, compared to RNA alone (Fig. S5, lanes 1, 3, and 4), confirming effective RNase L activation and subsequent RNA degradation. RNase L alone caused a ~20 % reduction in FAM intensity (Fig. S5, lane 2), likely due to the proximity between the enzyme and RNA. Interestingly, Ribo1-Cy5 induced a more substantial reduction in FAM intensity of about ~70 % (Fig. S5, lane 6), whereas Ribo2-Cy5 caused only a 17 % decrease (Fig. S5, lane 5), suggesting that Ribo1-Cy5 is a more potent recruiter for RNase L than Ribo2-Cy5. Incubation with the Cy5 control compound (Cy5-Ctrl) resulted in a ~20 % reduction in FAM intensity (Fig. S5, lane 7), which may similarly be attributed to RNA-RNase L proximity. These findings indicate that both Ribo1-Cy5 and Ribo2-Cy5 bind to and recruit RNase L effectively without compromising its catalytic function, thereby preserving its RNA degradation activity.

3.5. Novel fluorescent probes enable reliable visualization of RNase L localization in cells

One of the biggest challenges in studying RNase L, especially in cells, is to localize and observe this protein. As mentioned in several publications, immunofluorescence techniques for observing RNase L are not effective in cells [32,33]. To confirm that this method was not providing proper tracking of RNase L, we purchased several antibodies compatible with immunocytochemistry and tested them for RNase L cellular localization after checking the probes' toxicity in the MCF-7 cell line (Fig. S6). Consistent with published findings, we were unable to observe RNase L fluorescence using this method (Fig. S7). Therefore, after designing, evaluating the affinity of, and validating our probes, we used them to study RNase L subcellular localization in cells. First, we evaluated RNase L levels in several cell lines using Western blot analysis (Fig. S8) to validate that RNase L is sufficiently expressed in specific cell lines. We selected MDA-MB-231 and MCF-7 cell lines, which showed different levels of RNase L, to study its localization within the cells. These cells were treated with the fully validated Ribo1-Cy5 and Ribo2-Cy5 probes at three time points: 5 min, 2h, and 24h. To visualize the nucleus, we used DAPI staining (shown in blue, Fig. 5). We were able to observe the probe after just 5 min, but the best uptake was measured after 2 h for MCF-7 (Fig. 5A) and MDA-MB-231 (Fig. S9). After 24 h, no significant changes in probe distribution were observed (Figs. S9 and S10). As expected, we observed the probes primarily localized in the cytoplasm, consistent with the predominantly cytoplasmic localization of RNase L. Notably, both probes Ribo1-Cy5 and Ribo2-Cy5 showed similar distribution within the cells, strengthening our hypothesis that we are indeed observing RNase L.

To validate that RNase L was being observed, we designed and used an RNase L-GFP plasmid. After transfection of the reporter plasmid, we treated MCF-7 cells with the two Cy5 fluorescent probes and observed a high overlap of the fluorescent probes with the GFP signal, confirming that our probes are indicating RNase L subcellular localization (Fig. 5B). To quantify this co-localization, we calculated the Pearson's Correlation Coefficient (PCC) and observed a high PCC value of $r = 0.77$, indicating strong spatial correspondence (Fig. 5C). Collectively, we have successfully observed subcellular RNase L localization with our designed probes without any specific treatment, demonstrating clear distribution and rapid uptake. This method offers significant advantages over traditional immunofluorescence techniques or plasmid transfection, which cannot study endogenous RNase L in cells. Our approach provides a more reliable and efficient means of visualizing native RNase L in living cells.

3.6. Fluorescent probes demonstrate rapid, RNase L-dependent uptake across diverse cell lines

To further characterize our fluorescent probes for studying RNase L, we investigated their uptake kinetics across multiple cell lines expressing varying enzyme levels. Using fluorescence-activated cell sorting (FACS), we quantitatively assessed probe uptake based on cellular fluorescence intensity and concentration differences among the cell lines. Consistent with our subcellular localization assays, a significant increase in cellular fluorescence was detected after just 5 min of probe exposure. Notably, the fluorescence intensity reached its maximum after 2 h of treatment and remained comparable to measurements taken at 24 h post-exposure in MCF-7 and MDA-MB-231 cells (Fig. 6A), and HEK-293 cells (Fig. S11). This suggests rapid probe internalization and saturation. Since we observed similar uptake patterns in both MCF-7 and MDA-MB-231 cell lines, this indicates that probe internalization is not cell-type specific. This consistency across cell types supports the broad applicability of our probes for RNase L studies in diverse cellular contexts.

To further validate our approach, we compared fluorescence uptake among three cell lines known to express different levels of RNase L: MCF-7, MDA-MB-231, and HEK-293. Intriguingly, we found a positive correlation between probe uptake and RNase L expression levels (Fig. 6B). MCF-7 cells, which express the highest levels of RNase L, showed the greatest probe uptake, followed by HEK-293 cells, with MDA-MB-231 cells showing the lowest uptake. This correlation strongly suggests that our probes specifically target RNase L in cellular environments. These findings collectively demonstrate the efficiency, specificity, and versatility of our

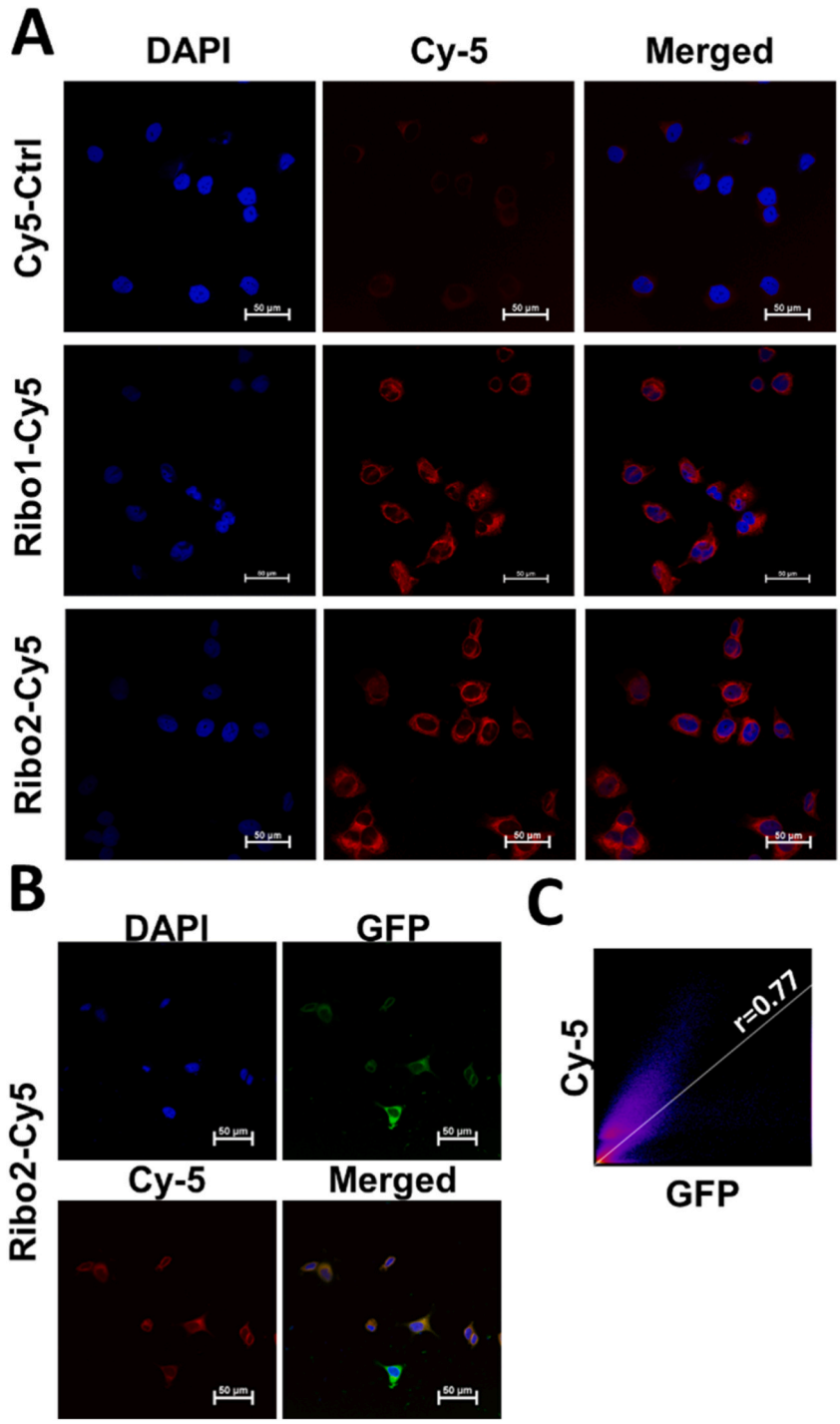

Fig. 5. Uptake of probes by MCF-7 cells and RNase L subcellular localization. A) Representative fluorescence images showing the cellular uptake of fluorescent probes Cy5-Ctrl (1 μM), Ribo1-Cy5 (1 μM), and Ribo2-Cy5 (1 μM) (red) with nucleus marker DAPI (blue), after 2 h treatment. Scale bar = 50 μm. B) Representative fluorescence images showing RNase L subcellular localization upon 2 h treatment with Ribo2-Cy5 (0.1 μM) (red), GFP tagged RNase L (green), and nucleus marker DAPI (blue). Scale bar = 50 μm. C) Scatter plot showing the relationship between fluorescent probes and RNase L localization; the solid line represents the best-fit regression line, illustrating the positive correlation ($r = 0.703 \pm 0.037$).

fluorescent probes for studying RNase L in living cells. The rapid uptake, cell-type independence, and correlation with RNase L expression levels underscore the potential of these probes as powerful tools for investigating RNase L dynamics and distribution in various cellular systems.

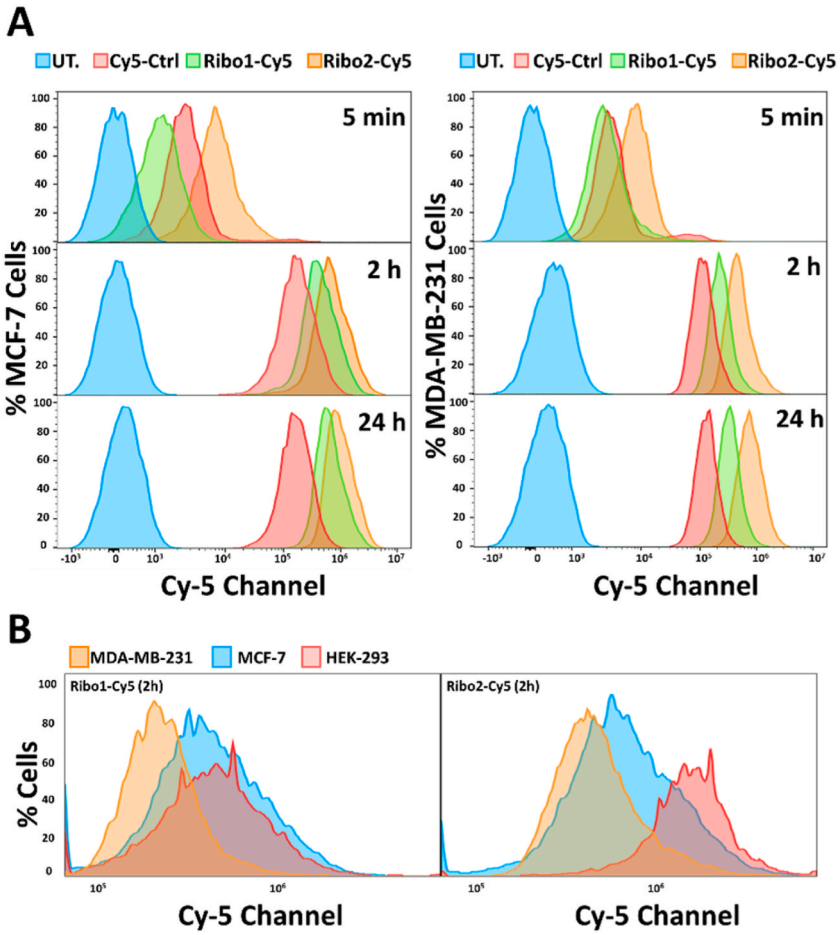

Fig. 6. Fluorescent probes cellular uptake in MCF-7 and MDA-MB-231 cell lines. A) Fluorescence-activated cell sorting assay after 5 min, 2 h, and 24 h treatment (1 μM). Cyan represents untreated cells, pink represents Cy5-Ctrl, green represents Ribo1-Cy5, and orange represents Ribo2-Cy5. B) Ribo1-Cy5 and Ribo2-Cy5 cellular uptake comparison among MDA-MB-231 (orange), MCF-7 (cyan), and HEK-293 (pink) after 2 h treatment (1 μM).

4. Discussion

Our study presents a significant advancement in the field of RNase L research through the development and characterization of novel fluorescent probes designed to bind and visualize this crucial enzyme. These probes, based on previously reported RNase L recruiters, offer several advantages over traditional methods for studying RNase L dynamics and localization in living cells. The synthesis of multiple fluorescent derivatives covering a broad spectrum of visible light provides a versatile toolkit for RNase L visualization. By conjugating RNase L recruiters with various fluorophores (Coumarin, Fluorescein, NBD, and Cy5), we have developed probes that can be applied in diverse experimental settings, allowing for multicolor imaging and compatibility with different microscopy techniques. The binding affinity assays demonstrated that our probes maintain a high affinity for RNase L, with EC_{50} values in the high picomolar range. This strong binding affinity ensures sensitive detection of RNase L in cellular environments. Moreover, the competitive binding assays validated that several of our probes, particularly the Cy5 derivatives and Ribo2-Cou, target the same binding pocket as the original RNase L binders. This confirmation is crucial for ensuring the specificity of our probes and their relevance to RNase L-related studies. One of the most significant achievements of this study is the successful visualization of endogenous RNase L in living cells, a feat that has been challenging with traditional immunofluorescence techniques. Our probes enabled the observation of RNase L subcellular localization without the need for genetic manipulation or cell fixation. The rapid uptake and clear cytoplasmic distribution of the probes align with the known localization of RNase L, providing a reliable method for studying its dynamics in real-time.

The correlation between probe uptake and RNase L expression levels across different cell lines further validates the specificity of our probes. This finding not only confirms the probes' utility in visualizing RNase L but also suggests their potential as tools for quantifying relative RNase L expression levels in various cell types. The advantages of our fluorescent probes over traditional methods are numerous. Unlike immunofluorescence, which often fails to detect RNase L effectively in cells, our probes offer high sensitivity and specificity. Compared to plasmid transfection methods, our approach allows for the study of endogenous RNase L, providing a more

physiologically relevant picture of its behavior and distribution. Additionally, we have demonstrated the probes' efficacy in several cell lines, though their performance in other cell types or *in vivo* models remains to be explored.

5. Conclusion

This study introduces innovative fluorescent probes for visualizing RNase L in living cells, addressing a significant challenge in the field. Our approach overcomes the limitations of traditional methods, enabling real-time observation of endogenous RNase L without genetic manipulation or cell fixation. These tools open new possibilities for investigating RNase L's role in antiviral defense and RNA regulation. The broad spectral range and specificity of our probes offer versatility for various experimental designs. Their potential extends beyond basic research, potentially aiding in the development of RIBOTACs and screening for RNase L modulators. While this work provides a solid foundation, future studies should explore the probes' applications in diverse cellular contexts and potential *in vivo* use. As we continue to unravel the complexities of RNase L biology, these tools may contribute to advancements in understanding innate immunity and developing RNA-targeted therapeutics.

6. Significance

This study represents a significant advancement in understanding RNase L, the crucial ribonuclease involved in the RIBOnuclease TArgeting Chimera (RIBOTAC) approach. Our tools fill critical gaps in existing methodologies for studying RNase L dynamics and RNA degradation pathways, which are key to antiviral defense and the development of RIBOTACs. By enabling real-time visualization of RNase L activity and intracellular localization, this work not only enhances our understanding of RNase L's role in RNA biology but also paves the way for more effective RNA-targeted therapies. The versatility of these fluorescent probes also supports high-throughput screening for RNase L modulators, potentially accelerating the discovery of novel therapeutic agents. This research, therefore, provides valuable tools for both fundamental studies and the clinical advancement of RNA-targeted treatments.

CRediT authorship contribution statement

Elias Khaskia: Visualization, Validation, Investigation, Formal analysis, Data curation. **Raphael I. Benhamou:** Writing – review & editing, Writing – original draft, Supervision, Funding acquisition, Formal analysis, Data curation, Conceptualization.

Data availability statement

General experimental details of biological evaluation, synthesis and characterization of new molecules are included in the manuscript and supporting information.

Declaration of competing interest

The authors declare that they have no known competing financial interests or personal relationships that could have appeared to influence the work reported in this paper.

Acknowledgments

Funding: The authors are funded by the Israel Cancer Research Fund (ICRF, 22-201-RCDA); the Israeli Centers for Research Excellence from the Council for Higher Education; the Israel Ministry of Innovation, Science and Technology (0004943); and the Israel Science Foundation (grant 1925/22). E.K. fellowship is funded by the Neubauer Fellows in the Sciences Scholarship.

Appendix A. Supplementary data

Supplementary data to this article can be found online at https://doi.org/10.1016/j.heliyon.2024.e41295.

References

[1] R.H. Silverman, Viral encounters with 2′,5′-oligoadenylate synthetase and RNase L during the interferon antiviral response, J. Virol. 81 (2007) 12720–12729, https://doi.org/10.1128/jvi.01471-07.

[2] D.A. Cooper, S. Banerjee, A. Chakrabarti, A. García-Sastre, J.R. Hesselberth, R.H. Silverman, D.J. Barton, RNase L targets distinct sites in influenza A virus RNAs, J. Virol. 89 (2015) 2764–2776, https://doi.org/10.1128/jvi.02953-14.

[3] Y. Li, S. Banerjee, Y. Wang, S.A. Goldstein, B. Dong, C. Gaughan, R.H. Silverman, S.R. Weiss, Activation of RNase L is dependent on OAS3 expression during infection with diverse human viruses, Proc. Natl. Acad. Sci. U. S. A. 113 (2016) 2241–2246, https://doi.org/10.1073/pnas.1519657113.

[4] Y. Li, D.M. Renner, C.E. Comar, J.N. Whelan, H.M. Reyes, F.L. Cardenas-Diaz, R. Truitt, L.H. Tan, B. Dong, K.D. Alysandratos, J. Huang, J.N. Palmer, N. D. Adappa, M.A. Kohanski, D.N. Kotton, R.H. Silverman, W. Yang, E.E. Morrisey, N.A. Cohen, S.R. Weiss, Sars-cov-2 induces double-stranded rna-mediated innate immune responses in respiratory epithelial-derived cells and cardiomyocytes, Proc. Natl. Acad. Sci. U. S. A. 118 (2021) e2022643118, https://doi.org/10.1073/pnas.2022643118.

[5] B. Dong, R.H. Stlvermanz, 2-5A-dependent RNase molecules dimerize during activation by 2-5A, J. Biol. Chem. 270 (1995) 4133–4137, https://doi.org/10.1074/jbc.270.8.4133.
[6] R.H. Silverman, J.J. Skehel, T.C. James, D.H. Wreschner, I.M. Kerr, rRNA cleavage as an index of ppp(A2'p)nA activity in interferon-treated encephalomyocarditis virus-infected cells, J. Virol. 46 (1983) 1051–1055, https://doi.org/10.1128/JVI.46.3.1051-1055.1983.
[7] Y. Han, J. Donovan, S. Rath, G. Whitney, A. Chitrakar, A. Korennykh, Structure of human RNase L reveals the basis for regulated RNA decay in the IFN response, Science 343 (2014) 1244–1248, https://doi.org/10.1126/SCIENCE.1249845.
[8] A. Chitrakar, S. Rath, J. Donovan, K. Demarest, Y. Li, R.R. Sridhar, S.R. Weiss, S.V. Kotenko, N.S. Wingreen, A. Korennykh, Real-time 2-5A kinetics suggest that interferons β and λ evade global arrest of translation by RNase L, Proc. Natl. Acad. Sci. U. S. A. 116 (2019) 2103–2111, https://doi.org/10.1073/pnas.181836311.
[9] A. Karasik, G.D. Jones, A.V. Depass, N.R. Guydosh, Activation of the antiviral factor RNase L triggers translation of non-coding mRNA sequences, Nucleic Acids Res. 49 (2021) 6007–6026, https://doi.org/10.1093/NAR/GKAB036.
[10] R. Cusic, J.M. Burke, Condensation of RNase L promotes its rapid activation in response to viral infection in mammalian cells, Sci. Signal. 17 (2024) 1–13, https://doi.org/10.1126/scisignal.adi9844.
[11] P. Manivannan, M. Siddiqui Adnan, K. Malathi, RNase L amplifies interferon signaling by inducing protein, J. Virol. 94 (2020) 1–21, https://doi.org/10.1128/JVI.00205-20.
[12] M.G. Costales, B. Suresh, K. Vishnu, M.D. Disney, Targeted degradation of a hypoxia-associated non-coding RNA enhances the selectivity of a small molecule interacting with RNA, Cell Chem. Biol. 26 (2019) 1180–1186.e5, https://doi.org/10.1016/J.CHEMBIOL.2019.04.008.
[13] M.G. Costales, Y. Matsumoto, S.P. Velagapudi, M.D. Disney, Small molecule targeted recruitment of a nuclease to RNA, J. Am. Chem. Soc. 140 (2018) 6741–6744, https://doi.org/10.1021/JACS.8B01233.
[14] L. Borgelt, N. Haacke, P. Lampe, X. Qiu, R. Gasper, D. Schiller, J. Hwang, S. Sievers, P. Wu, Small-molecule screening of ribonuclease L binders for RNA degradation, Biomed. Pharmacother. 154 (2022) 113589, https://doi.org/10.1016/j.biopha.2022.113589.
[15] S.M. Meyer, T. Tanaka, P.R.A. Zanon, J.T. Baisden, D. Abegg, X. Yang, Y. Akahori, Z. Alshakarchi, M.D. Cameron, A. Adibekian, M.D. Disney, DNA-encoded library screening to inform design of a ribonuclease targeting chimera (RiboTAC), J. Am. Chem. Soc. 144 (2022) 21096–21102, https://doi.org/10.1021/JACS.2C07217.
[16] M.G. Costales, H. Aikawa, Y. Li, J.L. Childs-Disney, D. Abegg, D.G. Hoch, S.P. Velagapudi, Y. Nakai, T. Khan, K.W. Wang, I. Yildirim, A. Adibekian, E.T. Wang, M.D. Disney, Small-molecule targeted recruitment of a nuclease to cleave an oncogenic RNA in a mouse model of metastatic cancer, Proc. Natl. Acad. Sci. U. S. A. 117 (2020) 2406–2411, https://doi.org/10.1073/PNAS.1914286117.
[17] N.A. Springer, S.M. Meyer, A. Taghavi, J.L. Childs-Disney, M.D. Disney, Small Molecules that Degrade RNA, RNA as a Drug Target, 2024, pp. 227–252, https://doi.org/10.1002/9783527840458.CH9.
[18] K. Tadesse, R.I. Benhamou, Targeting MicroRNAs with small molecules, Non-Coding RNA 10 (2024) 17, https://doi.org/10.3390/NCRNA10020017.
[19] Y. Tong, Y. Lee, X. Liu, J.L. Childs-Disney, B.M. Suresh, R.I. Benhamou, C. Yang, W. Li, M.G. Costales, H.S. Haniff, S. Sievers, D. Abegg, T. Wegner, T.O. Paulisch, E. Lekah, M. Grefe, G. Crynen, M. Van Meter, T. Wang, Q.M.R. Gibaut, J.L. Cleveland, A. Adibekian, F. Glorius, H. Waldmann, M.D. Disney, Programming inactive RNA-binding small molecules into bioactive degraders, Nature 618 (2023) 169–179, https://doi.org/10.1038/S41586-023-06091-8.
[20] J.M. Burke, N. Ripin, M.B. Ferretti, L.A. St Clair, E.R. Worden-Sapper, F. Salgado, S.L. Sawyer, R. Perera, K.W. Lynch, R. Parker, RNase L activation in the cytoplasm induces aberrant processing of mRNAs in the nucleus, PLoS Pathog. 18 (2022) e1010930, https://doi.org/10.1371/JOURNAL.PPAT.1010930.
[21] S. Haj-Yahia, A. Nandi, R.I. Benhamou, Targeted degradation of structured RNAs via ribonuclease-targeting Chimeras (RiboTacs), Expet Opin. Drug Discov. 18 (2023) 929–942, https://doi.org/10.1080/17460441.2023.2224960.
[22] H.S. Haniff, Y. Tong, X. Liu, J.L. Chen, B.M. Suresh, R.J. Andrews, J.M. Peterson, C.A. O'Leary, R.I. Benhamou, W.N. Moss, M.D. Disney, Targeting the SARS-COV-2 RNA genome with small molecule binders and ribonuclease targeting chimera (RiboTAC) degraders, ACS Cent. Sci. 6 (2020) 1713–1721, https://doi.org/10.1021/acscentsci.0c00984.
[23] M. Adane, M. Gebreyohannes, G. Gebreyohannes, A brief review on molecular diagnostic tools: principles, application and limitations, Adv. Biol. Res. 10 (2016) 388–397, https://doi.org/10.5829/IDOSI.ABR.2016.388.397.
[24] Y. Ueda, S. Kwok, Y. Hayashi, Application of FRET probes in the analysis of neuronal plasticity, Front. Neural Circ. 7 (2013) 64182, https://doi.org/10.3389/FNCIR.2013.00163/BIBTEX.
[25] N. Boonham, J. Kreuze, S. Winter, R. van der Vlugt, J. Bergervoet, J. Tomlinson, R. Mumford, Methods in virus diagnostics: from ELISA to next generation sequencing, Virus Res. 186 (2014) 20–31, https://doi.org/10.1016/J.VIRUSRES.2013.12.007.
[26] D. Wu, A.C. Sedgwick, T. Gunnlaugsson, E.U. Akkaya, J. Yoon, T.D. James, Fluorescent chemosensors: the past, present and future, Chem. Soc. Rev. 46 (2017) 7105–7123, https://doi.org/10.1039/C7CS00240H.
[27] H. Wang, X. Wang, P. Li, M. Dong, S.Q. Yao, B. Tang, Fluorescent probes for visualizing ROS-associated proteins in disease, Chem. Sci. 12 (2021) 11620–11646, https://doi.org/10.1039/D1SC02165F.
[28] S.H. Alamudi, Y.T. Chang, Advances in the design of cell-permeable fluorescent probes for applications in live cell imaging, Chem. Commun. 54 (2018) 13641–13653, https://doi.org/10.1039/C8CC08107G.
[29] E.C. Greenwald, S. Mehta, J. Zhang, Genetically encoded fluorescent biosensors illuminate the spatiotemporal regulation of signaling networks, Chem. Rev. 118 (2018) 11707–11794, https://doi.org/10.1021/ACS.CHEMREV.8B00333.
[30] C.S. Thakur, B.K. Jha, B. Dong, J. Das Gupta, K.M. Silverman, H. Mao, H. Sawai, A.O. Nakamura, A.K. Banerjee, A. Gudkov, R.H. Silverman, Small-molecule activators of RNase L with broad-spectrum antiviral activity, Proc. Natl. Acad. Sci. U. S. A. 104 (2007) 9585–9590, https://doi.org/10.1073/PNAS.0700590104.
[31] Y. Fu, N.S. Finney, Small-molecule fluorescent probes and their design, RSC Adv. 8 (2018) 29051–29061, https://doi.org/10.1039/C8RA02297F.
[32] A. Karasik, G.D. Jones, A.V. Depass, N.R. Guydosh, Activation of the antiviral factor RNase L triggers translation of non-coding mRNA sequences, Nucleic Acids Res. 49 (2021) 6007–6026, https://doi.org/10.1093/NAR/GKAB036.
[33] K. Ding, H. Li, F. Tai, J. Duan, Q. Wang, R. Zhai, H. Fu, C. Ge, X. Zheng, Unraveling the role of RNase L knockout in alleviating immune response activation in mice bone marrow after irradiation, Int. J. Mol. Sci. 25 (2024) 2722, https://doi.org/10.3390/IJMS25052722/S1.